Pusher-Propeller Installation Effects in Angular Inflow

Sinnige, Tomas; Ragni, Daniele; Eitelberg, Georg; Veldhuis, Leo

DOI
10.2514/6.2016-2875

Publication date
2016

Document Version
Accepted author manuscript

Published in
22nd AIAA/CEAS Aeroacoustics Conference

Pusher-Propeller Installation Effects in Angular Inflow

Tomas Sinnige*, Daniele Ragni†, Georg Eitelberg‡, and Leo L. M. Veldhuis§
Delft University of Technology, Delft, 2629 HS, the Netherlands

Pylon-mounted pusher propellers suffer from installation effects due to the interaction between the pylon and the propeller. The impact of angular inflow on these installation effects was quantified at the Large Low-Speed Facility of the German-Dutch wind tunnels (DNW-LLF). Particle-image-velocimetry measurements showed that the pylon wake's width and velocity deficit were hardly affected by the introduction of a six-degree sideslip angle. Application of pylon trailing-edge blowing reduced the integral velocity deficit in the wake by up to 65%. Evaluations of the surface pressures on the blades confirmed the sinusoidal loading behavior in angular inflow and the impulsive loading peak due to the pylon-wake encounter. The circumferential velocity components induced by the pylon tip vortex strongly affected the steady-state propeller performance by modifying the effective advance ratio sensed by the blades. Increased performance was measured when the rotation direction of the pylon tip vortex was opposite to that of the propeller. Angular inflow affected the propeller noise emissions due to the resulting unsteady blade loads and the circumferential variation of the effective Mach number of the blade sections. The installation of the pylon added a noise source due to the unsteady blade loads caused by the pylon-wake encounter. Depending on the sideslip angle, application of blowing eliminated a large part of the installation noise penalty, despite remaining non-uniformities in the blown wake profiles.

I. Introduction

MODERN design and manufacturing technologies have reestablished the propeller as an interesting alternative to turbofans in terms of maximum operating speed and specific thrust. At the same time, propellers offer a higher propulsive efficiency than turbofans because of their larger effective by-pass ratio. The resulting reduction in specific fuel consumption is the main driver behind today's research on propellers.

Interior-noise considerations, engine-integration issues, and mitigation of blade-loss risk motivate studies of propeller-aircraft lay-outs with rear-fuselage-mounted contra-rotating open rotors (CRORs).[1,2] In such a configuration, the propeller blades pass through the wake of the upstream pylon. This results in unsteady blade loads[3,4] and associated increased propeller noise emissions[5]. Investigations with CRORs have shown that these installation effects are dominated by the interaction between the pylon wake and the front rotor.[6–9] The adverse pylon-interaction effects can be mitigated by eliminating the momentum deficit in the pylon wake. This can be achieved using pylon blowing, as confirmed previously by experimental research with single-rotating[10–12] and contra-rotating[6–8,13] propellers, as well as numerical investigations[14].

In realistic flight scenarios, the inflow to the pylon–propeller combination is typically asymmetric. Yet, the literature on pusher-propeller installation effects mainly focuses on the symmetric-inflow case. A notable exception is the work by Magliozzi[15], who studied the pylon-installation effects for semi-installed propellers in both tractor and pusher configurations. It was shown that the installation of the pylon reduced the noise levels when operated at angle of attack, which was attributed to a flow-straightening effect of the pylon.

Apart from the lack of consideration of angular-inflow effects, existing experimental studies of the pylon-interaction phenomenon also do not contain evaluations of the unsteady blade loads. Nevertheless, these are crucial for the proper understanding of the acoustic behavior of the propeller. The experimental investigation discussed in the present paper aimed at filling these gaps. Moreover, it provided a first assessment of the

*Ph.D. Candidate, Flight Performance and Propulsion Section, Faculty of Aerospace Engineering, AIAA member.
†Assistant Professor, Wind Energy Section, Faculty of Aerospace Engineering, AIAA member.
‡Full Professor, Flight Performance and Propulsion Section, Faculty of Aerospace Engineering, AIAA member.
§Full Professor, Head of Flight Performance and Propulsion Section, Faculty of Aerospace Engineering, AIAA Member.

effects of pylon trailing-edge blowing under asymmetric inflow conditions. The propeller noise emissions were analyzed both at the source and in the far-field, by evaluating the unsteady blade loads and in-flow microphone recordings.

II. Methodology

A. Wind Tunnel Facility and Models

The experimental campaign was conducted at the Large Low-Speed Facility of the German-Dutch wind tunnels (DNW-LLF). In the selected open-jet configuration, the tunnel with outlet of 8 m x 6 m allows a wind speed range of $0 - 80$ m/s. At the selected free-stream velocity of 60 m/s, the turbulence level in the longitudinal direction is less than 0.24%, while the spatial total-pressure deviations are smaller than 0.1% in the core of the jet. The application of acoustic lining resulted in a semi-anechoic test environment. A fixed structure was installed in the test hall to support the propeller and pylon and provide yaw control of the entire setup. Figure 1 provides a photograph of the measurement setup.

An installed pusher-propeller configuration was simulated by positioning a powered tractor-propeller model downstream of a pylon equipped with a trailing-edge blowing system, as shown in Fig. 2. The propeller was previously used for the European APIAN (Advanced Propulsion Integration Aerodynamics and Noise)[16–19] project. It featured six highly swept carbon-fiber blades, with a rotor diameter of 0.508 m. The pylon model was manufactured by extrusion of a NACA 0010 profile into a straight, untapered wing of 0.489 m chord and 0.900 m span. The integration of the trailing-edge blowing system into the aft part of the model required an increase in trailing-edge thickness to 0.8% of the chord. The pylon was positioned upstream of the propeller at a fixed spacing of approximately 30% of the propeller diameter.

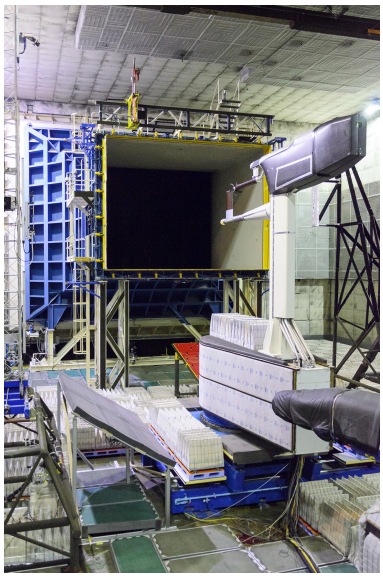

Figure 1. Overview of the experimental setup.

Figure 2. APIAN propeller installed downstream of the pylon model.

B. Experimental Techniques

Stereoscopic particle-image velocimetry (sPIV) was used to quantify the velocity deficit in the flow downstream of the pylon with and without the blowing system enabled. The measurements were performed in six horizontal planes downstream of the pylon, as illustrated in Fig. 3.

The integral propeller loads were measured during the entire test campaign with a rotating shaft balance, mounted on the motor shaft together with the propeller model. Additionally, local blade-loading information was obtained using surface-pressure transducers integrated into the propeller blades. This paper discusses the results measured using the fourteen sensors available at a radial station of $r/R \approx 0.65$, equally distributed over the pressure and suction sides of the blades. The pressure transducers covered a chordwise range of 5% to 90% of the local blade chord.

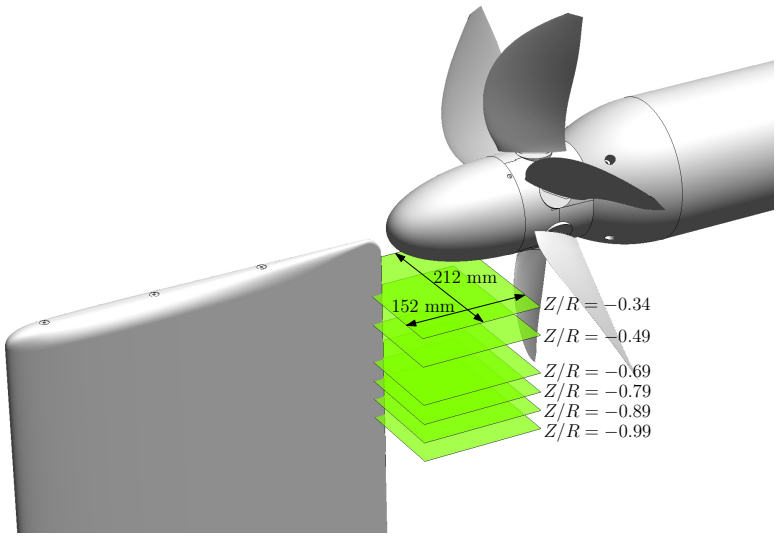

Figure 3. Positions of the sPIV measurement planes.

Figure 4. In-flow microphone wing.

In-flow microphones were used to assess the acoustic behavior of the propeller model. The measurement system, provided by Airbus[8], consisted of 39 microphones installed in the wing-shaped structure shown in Fig. 4. The complete system was traversed through the test hall in axial direction to cover an axial directivity range of $30° \leq \theta \leq 150°$, while allowing simultaneous measurements at circumferential directivity angles of $57° \leq \phi \leq 111°$. The definitions of the directivity angles θ and ϕ are provided in Fig. 5. Throughout the paper the emission angles are considered, not the geometric angles. The circumferential angle ϕ is also used to define the blade position in the discussion of the aerodynamic performance measurements.

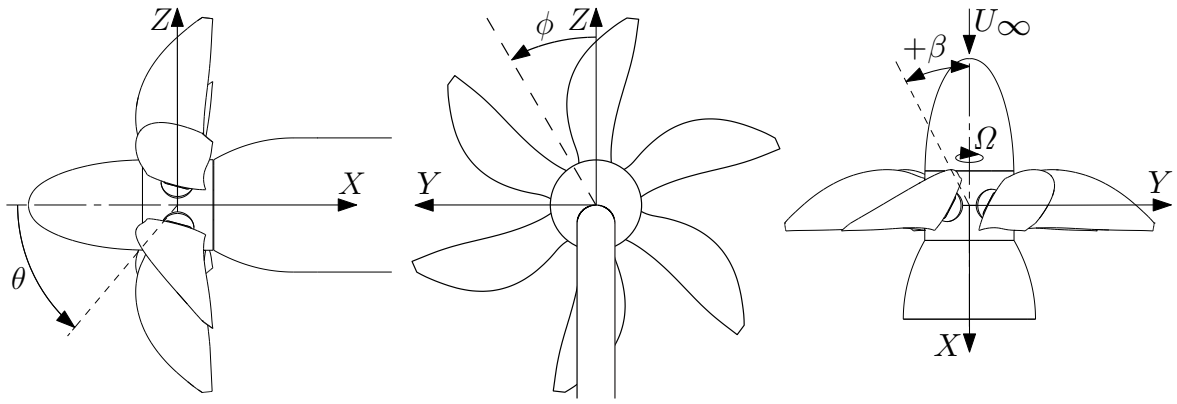

Figure 5. Coordinate-system definitions.

C. Analyzed Test Cases

All tests discussed in the present paper were performed at a free-stream velocity of $U_\infty = 60$ m/s. Measurements were taken mainly at three advance ratios, corresponding to low ($J = 1.75$), intermediate ($J = 1.40$), and high ($J = 1.05$) thrust settings. The associated values of the thrust coefficient ($C_T = \frac{T}{\rho_\infty n^2 D^4}$) equaled 0.18, 0.36, and 0.51, respectively. The effects of inflow asymmetries were analyzed by taking measurements at 0° and ±6° of sideslip angle, defined positive as in Fig. 5. Three different blowing rates were considered for the measurements with blowing enabled. The nominal rate was selected based on trial runs performed before the start of the final measurement program. The noise emissions were recorded using out-of-flow microphones for a range of blowing settings at a constant propeller operating point ($J = 1.40$, $\beta = 0°$). The blowing rate leading to the largest noise reductions was selected for the final test program, together with rates equal to 85% and 115% of this optimum. A blowing coefficient was introduced as the ratio between the blown mass flow and an equivalent free-stream mass flow referenced to the outflow area of the blowing slit. The optimal blowing rate corresponded to a blowing coefficient of $c_{\dot{m}} = 1.6$.

III. Results

A. Propeller Inflow

The momentum deficit in the pylon wake is the main cause of the pylon–propeller interaction effects occurring for pusher propellers. Figure 6 compares the velocity fields acquired downstream of the unblown pylon, for symmetric and asymmetric inflow conditions. The measurements were taken at 69% of the propeller radius below the propeller axis ($Z/R = -0.69$). The propeller was operated at the low-thrust condition ($J = 1.75$). Note that for the asymmetric case both the pylon and propeller were rotated relative to the incoming wind, while the orientation of the sPIV plane was not changed. The dashed lines in Fig. 6 are parallel to the propeller plane, at an upstream distance from the propeller of approximately 8% of the rotor diameter. The asterisks indicate the intersection between the dashed lines and the propeller axis.

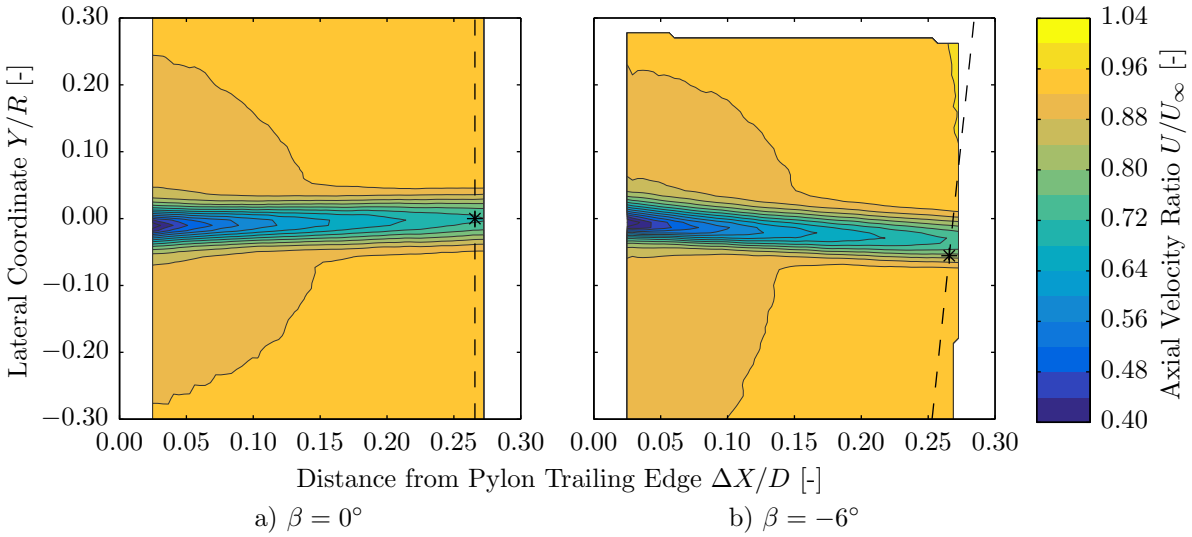

Figure 6. Effect of angular inflow on the velocity fields downstream of the pylon; $Z/R = -0.69$, $J = 1.75$.

The contours of the axial velocity presented in Fig. 6 display the expected trends. The pylon wake followed the rotation of the pylon, and the angular inflow introduced an asymmetry into the propeller suction. Figure 7 presents the velocity profiles extracted along the dashed lines indicated in Fig. 6, positioned at 8% of the rotor diameter upstream of the propeller ($\Delta X_\mathrm{p}/D = 0.08$). Apart from the unblown results, Fig. 7 also contains the inflow profiles obtained at the three different blowing coefficients for the case at sideslip. The results obtained for the symmetric configuration with blowing enabled were discussed before in Ref. 12 and hence are omitted here. A wake-based coordinate Y_w was defined to indicate the lateral position in the pylon wake, as illustrated in the sketch on the right of Fig. 7.

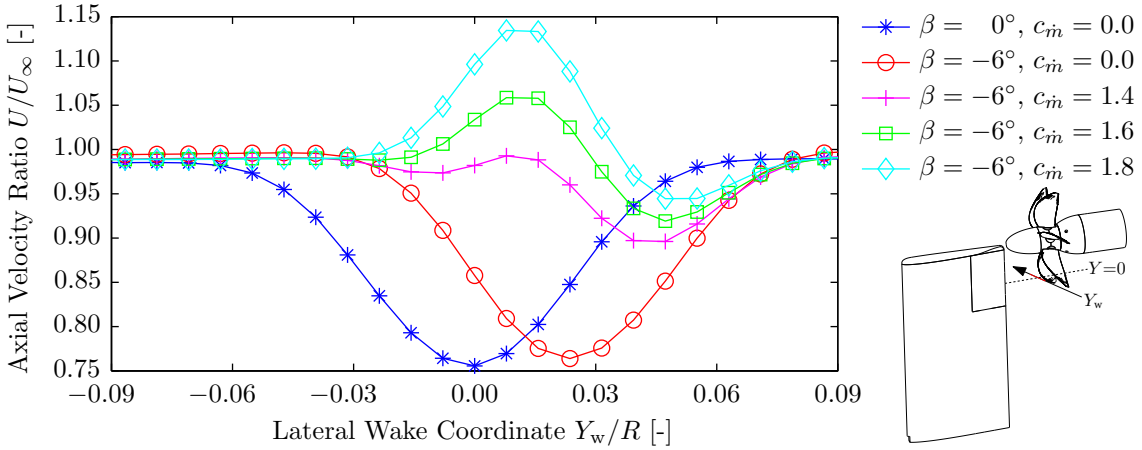

Figure 7. Propeller inflow versus sideslip angle and blowing coefficient; $\Delta X_\mathrm{p}/D = 0.08$, $Z/R = -0.69$, $J = 1.75$.

Figure 7 shows that the wake profiles were shifted away from the pylon–propeller axis due to the angular inflow. The wake width and velocity deficit were however not significantly affected by the operation at non-zero sideslip. The trailing-edge blowing system did not completely fill the pylon wake because of the asymmetric nature of the wake at sideslip. Instead, a velocity overshoot occurred in one half of the wake, while in the other half a velocity deficit remained. Nonetheless, application of the blowing system still reduced the integral magnitude of the velocity deficit in the wake region by around 65% at the optimal blowing rate ($c_{\dot{m}} = 1.6$). To achieve better performance in angular inflow conditions, a blowing system would be required with an outlet integrated along the chord on each side of the pylon.

B. Propeller Performance

Operation of the propeller at non-zero incidence to the incoming flow causes unsteady blade loading. Installation of the pylon introduces an additional cyclic perturbation, experienced by the blades as a periodic increase of the angle of attack during the pylon-wake passage.

1. Isolated Configuration

For the isolated propeller, operation in angular inflow results in unsteady blade loading of sinusoidal nature. Considering the symmetry of the isolated propeller configuration, the aerodynamic effects due to angle of attack and sideslip are equivalent. Figure 8 presents the development of the sectional blade lift coefficient at $r/R \approx 0.65$ for the isolated propeller operated at sideslip angles of 0° and ±6°. The results were obtained by averaging over multiple data points, each containing approximately 2,000 to 3,400 revolutions, depending on the rotational speed of the propeller. The circumferential blade position ϕ was defined relative to the leading edge of the blade at $r/R \approx 0.65$. For clarity, markers are displayed at fifteen-degree intervals.

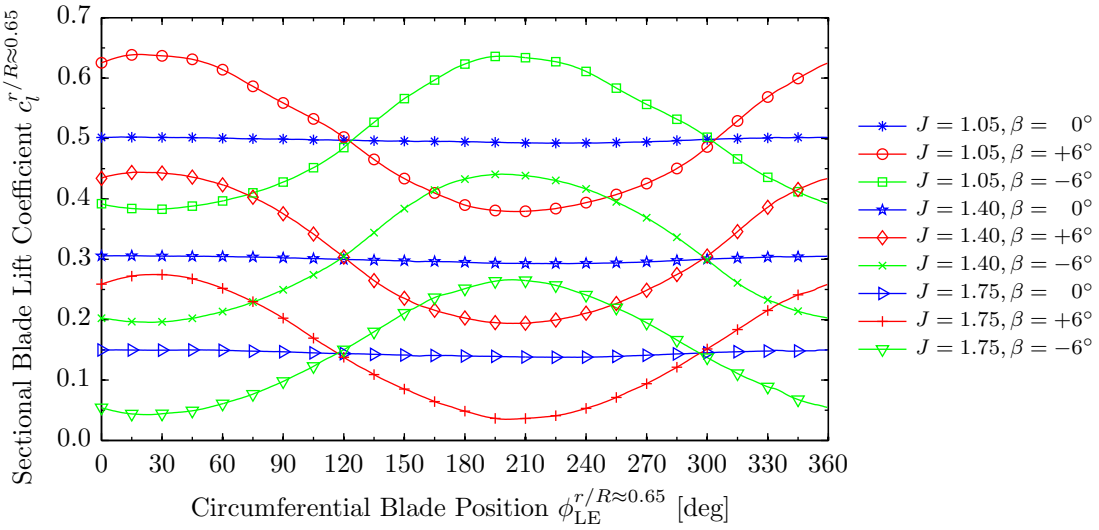

Figure 8. Effect of angular inflow on the propeller blade loading at $r/R \approx 0.65$; isolated propeller.

Figure 8 confirms the expected sinusoidal behavior of the sectional lift at sideslip angles of ±6°. The results at positive and negative sideslip were equivalent, only shifted by a phase offset of 180°. At positive sideslip, the blades experienced increased loads in the upper part of the disk ($\phi \approx 0°$) due to the local increase in effective rotational speed, while the opposite occurred at negative sideslip. The measurements taken under symmetric inflow conditions also showed a slight one-per-revolution oscillation, corresponding to an inflow angularity of approximately 0.2°. This is expected to be the result of a flow perturbation introduced by the in-flow measurement infrastructure. Also, it could have been due to a slight misalignment of the test setup.

Integrated over the entire rotation, the modification of the blade loads by the angular inflow was only significant at the medium and low thrust settings ($J = 1.40$ and $J = 1.75$), with an increase in mean loading of 5% when operated at sideslip. This is because the increase in loading in one half of the disk had a larger magnitude than the decrease in loading in the opposite part of the rotation. To verify whether this increase in local loading led to increased propeller thrust, Table 1 provides the thrust coefficients measured with the rotating shaft balance at the same operating conditions as considered in Fig. 8.

Table 1. Effect of angular inflow on the time-averaged propeller thrust coefficient; isolated propeller.

J	$C_T^{\beta=0^\circ}$	$C_T^{\beta=+6^\circ}$	$C_T^{\beta=-6^\circ}$	$\Delta C_T^{\beta=+6^\circ}$	$\Delta C_T^{\beta=-6^\circ}$
1.05	0.509 ± 0.001	0.510 ± 0.001	0.510 ± 0.001	+0.3%	+0.3%
1.40	0.356 ± 0.004	0.362 ± 0.004	0.362 ± 0.004	+1.7%	+1.5%
1.75	0.184 ± 0.008	0.187 ± 0.008	0.188 ± 0.008	+1.4%	+2.0%

Table 1 shows that the difference in propeller thrust between the cases with symmetric and asymmetric inflow was small. Depending on the advance ratio, the thrust increased by up to 2% due to the introduction of the sideslip angle. However, the measured increase in thrust coefficient did not exceed the measurement variability at any of the thrust settings considered. As expected, the results obtained at $\beta = +6^\circ$ and $\beta = -6^\circ$ were equivalent.

2. Installed Configuration

With the pylon present in the flow field, the blade sections experience a periodic, impulsive increase in angle of attack during the wake encounter. This is due to the momentum deficit in the pylon wake, which leads to a reduced inflow velocity to the blades when passing through the wake. In asymmetric inflow, this effect is superimposed on the sinusoidal load variations due to the angle-of-incidence effects discussed earlier. To evaluate the impact of the installation of the pylon on the local blade response, Fig. 9 compares the phase-averaged time histories of the sectional lift coefficient at $r/R \approx 0.65$ for the isolated and installed configurations, with and without sideslip. Only the low-thrust case, corresponding to $J = 1.75$, is considered. Markers are again displayed at fifteen-degree intervals.

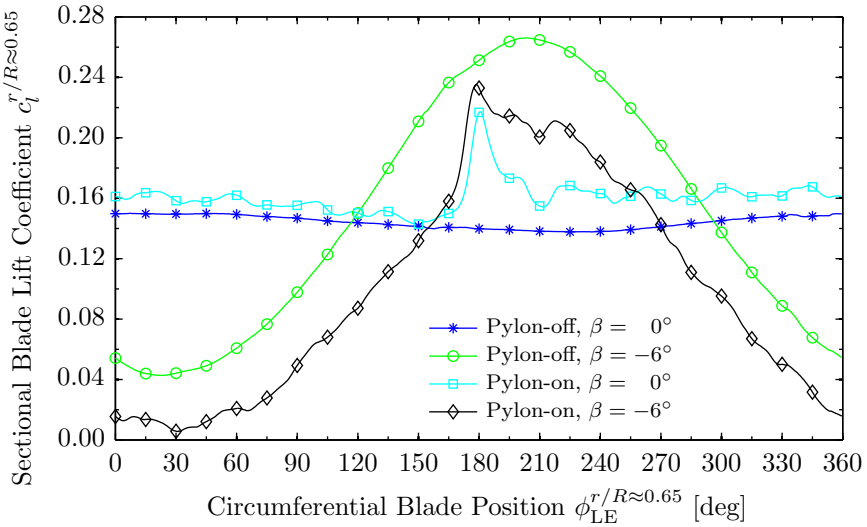

Figure 9. Effect of angular inflow and pylon installation on the propeller blade loading at $r/R \approx 0.65$; $J = 1.75$.

Figure 9 highlights the difference between the modification of the blade response due to the angular inflow on the one hand and the presence of the pylon on the other. Whereas the angle-of-incidence effect resulted in a loading oscillation with a period of one full rotation, the installation of the pylon led to an impulsive change in the blade lift during the wake passage. The corresponding strong pressure gradients cause increased far-field noise levels, as discussed later. The impact of the pylon wake on the blade loads was comparable for the cases in symmetric and asymmetric inflow.

Outside of the wake region, the effect of the pylon on the blade response was small but significant for the symmetric case. When operated in angular inflow, on the other hand, the blade loading decreased by about four to eight lift counts throughout the rotation due to the presence of the pylon. Table 2 illustrates the effect of this shift in blade loads on the integral propeller performance. Note that apart from the offset in loading, the shapes of the pylon-off and pylon-on curves were comparable. Therefore, it is concluded that the flow-straightening effect mentioned in Ref. 15 did not occur in the current experiments.

Table 2. Effect of angular inflow on the time-averaged propeller thrust coefficient; installed configuration.

J	$C_T^{\beta=0^\circ}$	$C_T^{\beta=+6^\circ}$	$C_T^{\beta=-6^\circ}$	$\Delta C_T^{\beta=+6^\circ}$	$\Delta C_T^{\beta=-6^\circ}$
1.05	0.510 ± 0.001	0.567 ± 0.001	0.464 ± 0.001	$+11\%$	-9%
1.75	0.187 ± 0.008	0.281 ± 0.008	0.119 ± 0.008	$+51\%$	-36%

Table 2 shows that in asymmetric inflow conditions the propeller thrust was strongly affected by the installation of the pylon. This was due to the circumferential velocity components induced by the pylon tip vortex, causing a constant change in blade-section angle of attack during the whole rotation. Effectively, the interaction with the pylon tip vortex modified the advance ratio experienced by the propeller blades. Depending on the direction of the sideslip angle, either positive or negative, the pylon tip vortex rotated in the opposite or same direction as the propeller. Correspondingly, the blade-section angles either increased or decreased, resulting in the large changes in propeller performance shown in Fig. 9 and Table 2. The tests at positive sideslip angle corresponded to a pitch-up attitude for an inboard-up rotating propeller on a realistic aircraft configuration. For this case, a given thrust could be achieved at a reduced rotational speed when compared to the isolated propeller configuration, thereby providing both efficiency and noise benefits. A similar conclusion was drawn by Patterson[20] based on experiments performed with a wing-tip-mounted pusher propeller. The absence of a dummy nacelle at the tip of the pylon might have strengthened the observed effects in the current test campaign.

3. Blown Configuration

As confirmed by Fig. 7, pylon blowing can be used to reduce the velocity deficit in the pylon wake. In this way, the inflow perturbations experienced by the propeller are decreased, thereby alleviating the impact of the installation effects. Figure 10 plots the phase-averaged sectional lift coefficient data measured in angular inflow, for the isolated and installed configurations with and without blowing. Three blowing rates are considered to illustrate the sensitivity of the blade response to the degree of wake filling. Markers are plotted at fifteen-degree intervals for clarity.

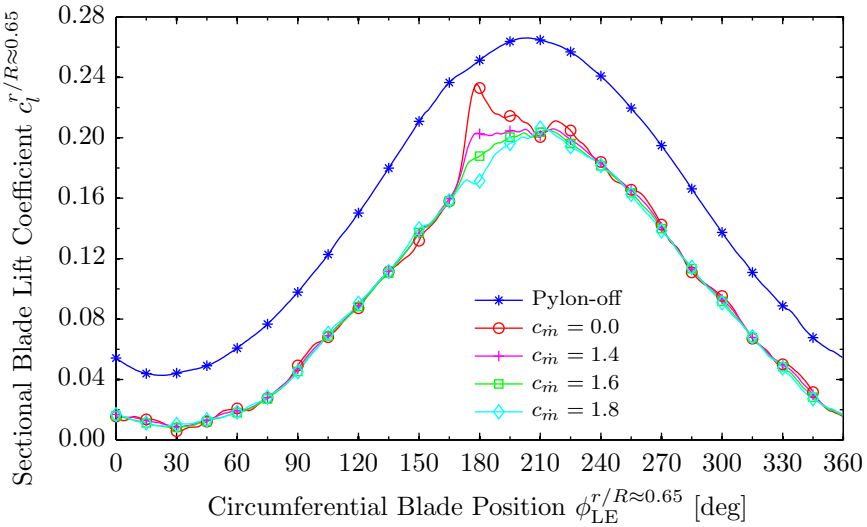

Figure 10. Effect of pylon blowing on the propeller blade loading at $r/R \approx 0.65$; $\beta = -6^\circ$, $J = 1.75$.

Figure 10 demonstrates the efficacy of the pylon-blowing system in reducing the unsteady blade loads. Despite the remaining non-uniformities in the wake profiles (Fig. 7), the application of blowing significantly reduced the impact of the installation effects. For the unblown configuration, the increase in lift coefficient during the wake passage was approximately six lift counts when compared to the response that would have been obtained without pylon wake. With blowing enabled, this was reduced to less than one lift count at the best-performing setting ($c_{\dot{m}} = 1.6$). Comparing the results obtained at the different blowing rates, it is concluded that the blade response showed a strong dependence on the non-uniformity of the inflow. At the lowest blowing rate, $c_{\dot{m}} = 1.4$, the momentum deficit in the pylon wake was not sufficiently filled yet, hence the effect of the increased angle of attack in the wake region was still present. At the highest blowing rate, on the other hand, the velocity overshoot in the wake caused a local reduction of the blade loads.

C. Propeller Noise Emissions

Besides the noise emissions due to blade thickness and steady loading, the unsteady blade loads discussed in the previous section introduce additional sources of propeller noise. Moreover, for the case of angular inflow the radiation efficiency varies throughout the rotation due to the fluctuating blade Mach number.[21] Throughout this section, comparisons are made between the results measured at the three sideslip angles. It should be noted that at a given advance ratio, the propeller thrust coefficients were significantly different between the three configurations, as discussed before in relation to Table 2.

1. Isolated Configuration

The in-flow microphone data were used to assess the sensitivity of the propeller noise emissions to the sideslip angle. Phase-averaging was performed to extract the periodic components from the microphone signals, after which bandpass filters were applied around the frequencies corresponding to integer multiples of the blade-passage frequency (BPF). The tonal noise levels were then computed as the root-mean-square amplitudes of the resulting acoustic-pressure waveforms. The microphone corresponding to an axial emission angle of $\theta_e = 90°$ was considered. Figure 11 plots the extracted tonal noise levels versus advance ratio for the three sideslip-angle cases.

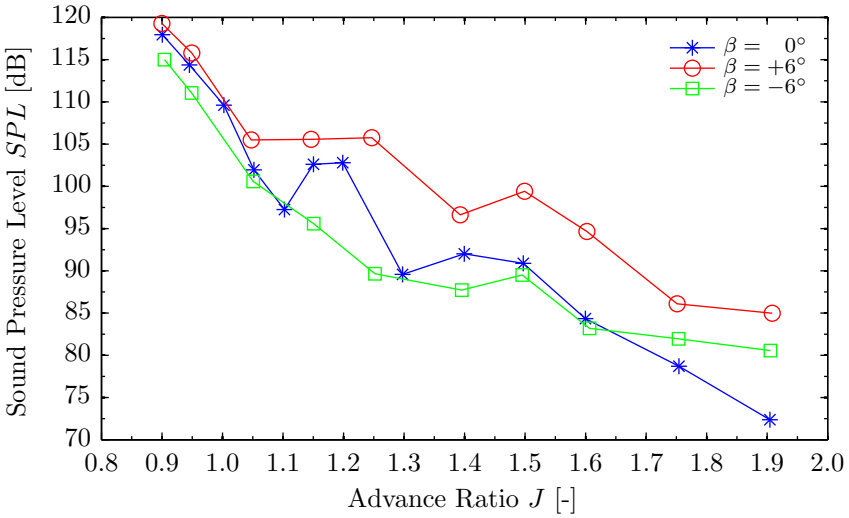

Figure 11. Effect of angular inflow and thrust setting on the isolated propeller's noise levels; $\theta_e = 90°$, $\phi = 90°$.

The results presented in Fig. 11 highlight the competing mechanisms introduced by the operation of the propeller in angular inflow. At the high thrust settings, corresponding to low advance ratios, the effects due to the fluctuating blade Mach number were dominant. The positive-sideslip case ($\beta = +6°$) corresponded to the situation with increased Mach numbers of the blade sections when rotating towards the microphones. Therefore, in the high-thrust regime the noise levels were highest at $\beta = +6°$ and lowest at $\beta = -6°$. The cyclic loads due to the asymmetric inflow became important at low thrust, when the amplitude of the steady-loading noise was small. This is observed for advance ratios below approximately 1.6, where the noise levels for the negative-sideslip case increased beyond those measured for the symmetric configuration. For all cases, the development of the sound pressure level with advance ratio was less smooth than expected. Analysis of the waveforms of the acoustic pressure showed that this was due to complex interference between the various noise sources.

2. Installed Configuration

The impulsively fluctuating blade loads during the wake passage cause additional noise emissions due to the associated unsteady blade pressures. Figure 12 presents the sound spectra measured using the in-flow microphone at a circumferential directivity angle of $\phi = 90°$, at an axial position corresponding to an emission angle in the propeller plane ($\theta_e = 90°$). An intermediate propeller thrust setting is considered, in this case corresponding to an advance ratio of $J = 1.50$. At this operating point, the trends in blade loading versus sideslip angle will be comparable to the results shown for $J = 1.40$ in Fig. 8.

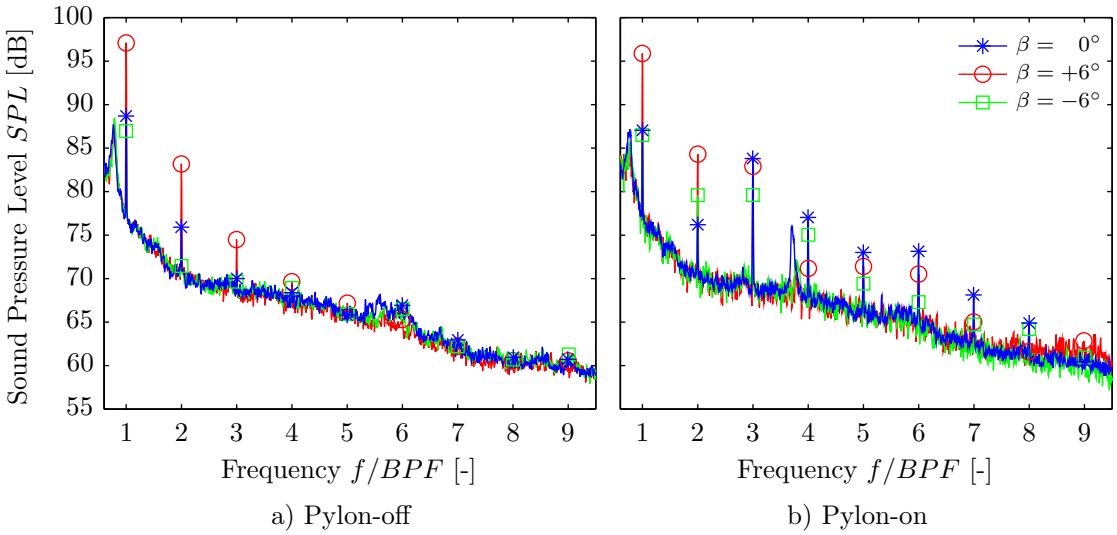

Figure 12. Effect of angular inflow on the propeller noise levels; $J = 1.50$, $\theta_e = 90°$, $\phi = 90°$.

The sound spectra plotted for the isolated configuration in Fig. 12a confirm the discussion under Fig. 11. Similar trends can be seen in Fig. 12b for the installed configuration, with increased tonal noise emissions for the positive-sideslip case and in general slightly reduced levels for the measurements at negative sideslip. Compared to the isolated configuration, the installation of the pylon only increased the tonal noise levels for the zero- and negative-sideslip cases. The broadband noise levels were only affected by the angular inflow for the pylon-installed configuration, with a slight increase in levels observed at high frequencies at $\beta = +6°$. This is attributed to the increased propeller loading due to the interaction with the pylon tip vortex as discussed earlier. The peak at 3.7 times the BPF for the symmetric case was due to vortex shedding from the pylon trailing edge.

The acoustic effects of operation at sideslip and installation of the pylon can be represented by summing the sound pressure levels of the various propeller tones. Figure 13 plots the resulting data for the isolated and installed configurations at the three sideslip angles considered.

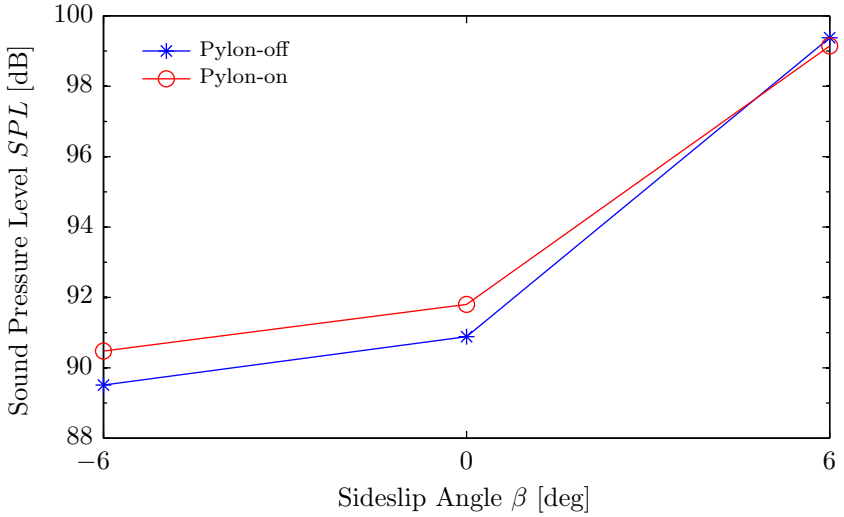

Figure 13. Effects of angular inflow and pylon installation on the tonal noise levels; $J = 1.50$, $\theta_e = 90°$, $\phi = 90°$.

Figure 13 shows that operation at positive sideslip amplified the propeller noise by 8 dB for the isolated configuration. Introduction of a negative sideslip angle, on the other hand, decreased the noise levels by 1.5 dB. This asymmetry in the impact of the angular inflow is due to the competing mechanisms discussed before. For the positive-sideslip case, the unsteady blade loads and asymmetric radiation-efficiency effects both increased the noise levels. At the negative sideslip angle, on the other hand, the unsteady blade loads increased the levels, which was however offset by the reduction in radiation efficiency towards the microphone.

Similar trends were observed for the pylon-installed configuration. Again, the highest noise levels occurred at the positive sideslip angle and the lowest at the negative sideslip angle, following the same physical reasoning as discussed before. However, the impact of the installation of the pylon was markedly different for the positive-sideslip case. At $\beta = -6°$ and $\beta = 0°$, the noise penalty due to pylon installation was approximately constant at 1 dB. For the $\beta = +6°$ case, on the other hand, the noise levels were slightly lower for the pylon-installed case than for the pylon-off configuration. The reason for this difference in the noise penalty due to pylon installation with the sideslip angle can possibly be traced back to the blade-loading distributions. Regardless of the sideslip angle, the pylon-installation impact was manifested as a sudden local increase of the blade loads. For the $\beta = 0°$ and $\beta = -6°$ cases, this increase added to an already positive loading gradient. At $\beta = +6°$, on the other hand, the angle-of-incidence effect led to a negative loading gradient in the region of the pylon-wake encounter. This resulted in an additional negative pressure peak in the acoustic-pressure signatures, reducing the overall noise levels. This highlights the importance of proper consideration of the effects due to asymmetric inflow in propeller-integration studies.

3. Blown Configuration

Having confirmed the impact of the installation of the pylon on the propeller noise levels, now the beneficial effects of pylon trailing-edge blowing are evaluated. In the remainder, the operating point corresponding to the low thrust setting ($J = 1.75$) is considered. Figure 14 plots the change in tonal noise emissions relative to the values measured for the isolated propeller as a function of the blowing coefficient. Again, the three sideslip cases are included, corresponding to $\beta = 0°$ and $\beta = \pm 6°$.

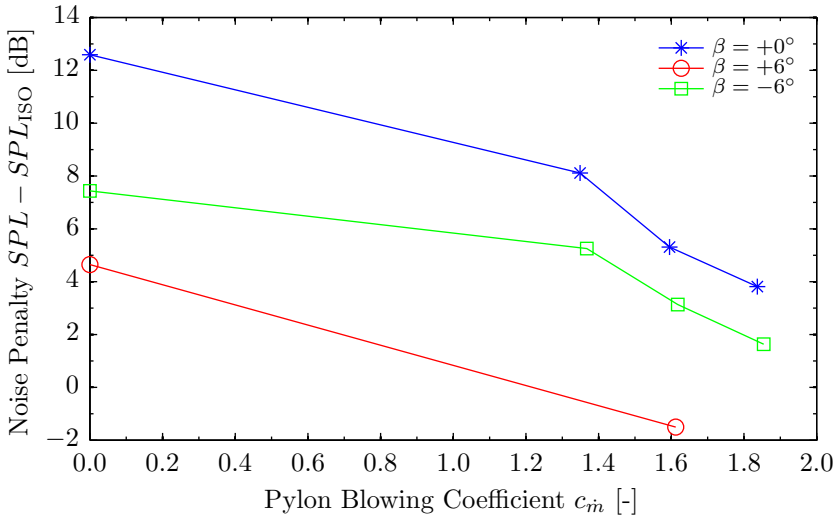

Figure 14. Effect of angular inflow and pylon blowing on the installation noise penalty; $J = 1.75$, $\theta_e = 90°$, $\phi = 90°$.

It can be seen in Fig. 14 that the pylon-installation effects were different at the low thrust setting than at the medium-thrust condition considered in Fig. 13. The noise penalty was especially large at $\beta = 0°$, with an increase of almost 13 dB for the unblown pylon-installed configuration. At $\beta = -6°$, the noise levels increased by about 7.5 dB, while at $\beta = +6°$ the noise penalty was even lower at 4.5 dB. This was due to the different ratio of steady and unsteady blade loads for the three inflow regimes, as observed before in Fig. 11. At sideslip, the noise emissions of the isolated propeller were higher than for the symmetric case, with noise increases of 7 dB and 3 dB at $\beta = +6°$ and $\beta = -6°$, respectively. As a result, the relative impact of the additional noise source due to the pylon installation was smaller for the two sideslip cases than for the symmetric configuration.

Application of the blowing system reduced the noise penalty due to the installation of the pylon at all inflow angles. In symmetric inflow conditions, the largest noise benefits were obtained at the highest blowing rate, with a remaining noise penalty of around 4 dB compared to the isolated propeller case. Note that these results differ from those presented in Ref. 12 for an intermediate thrust setting ($J = 1.40$). At the low-thrust condition considered in the current paper, the amplitude of the steady-loading noise was relatively small. Therefore, the noise associated with the remaining load fluctuations in the pylon-wake region had

sufficient amplitude to increase the overall sound pressure level. As a result, the lowest noise levels were not obtained for the blowing rate leading to the largest reduction of the integral velocity deficit in the pylon wake ($c_{\dot{m}} = 1.6$). Instead, the smallest noise penalty was observed at the blowing rate introducing a velocity overshoot on the wake centerline ($c_{\dot{m}} = 1.8$), leading to local unloading of the blades.

For the cases at sideslip, the remaining noise penalties due to the pylon installation with blowing enabled were smaller than at $\beta = 0°$. At $\beta = +6°$, the angular-inflow effects were relatively strong for the isolated propeller, as discussed before. Consequently, the reduction of the unsteady blade loads by blowing was sufficient to eliminate the noise penalty due to the installation of the pylon. As a result, the entire noise penalty due to the pylon-wake encounter had vanished at a blowing coefficient of $c_{\dot{m}} = 1.6$. In fact, the noise levels measured for the blown configuration were lower than for the isolated propeller. This was due to favorable interference between the various noise sources occurring for this case. The negative-sideslip case still featured a noise penalty with blowing enabled. The smaller noise penalty than at $\beta = 0°$ was as expected considering the higher noise level associated with the isolated propeller in this configuration (Fig. 11), which masked the noise due to the pylon-installation effects.

IV. Conclusions

The effects of angular inflow on the aerodynamic and aeroacoustic impact of pylon installation have been assessed for a pusher-propeller configuration. Based on the experimental results, the following conclusions were drawn:

- The pylon wake is hardly affected by operation of the pylon–propeller combination at a sideslip angle of six degrees. Compared to the situation for symmetric inflow conditions, the integrated velocity deficit did not increase due to the angular inflow. Application of pylon trailing-edge blowing in angular inflow results in an asymmetric wake velocity profile, with a velocity overshoot in one half of the wake and a velocity deficit in the other. At the optimal blowing rate, a reduction in integrated velocity deficit of approximately 65% was obtained compared to the unblown configuration.

- Operation of the isolated propeller at angle of incidence leads to a sinusoidal variation of the blade loads during each revolution. At medium and low thrust settings, this increased the mean blade lift by 5%. With the pylon present, two additional installation effects occur. The momentum deficit in the pylon wake causes a local, impulsive change in blade loading during the wake passage. Moreover, the circumferential velocity components induced by the pylon tip vortex result in a constant offset in blade loading throughout the rotation. The propeller performance is increased if the sense of rotation of the propeller is opposite to that of the pylon tip vortex.

- The noise emissions of the isolated propeller are affected by the angular inflow in two ways. The unsteady blade loads introduce an additional noise source, while also a circumferential variation of the radiation efficiency occurs due to the fluctuating Mach numbers of the blade sections. The noise levels are amplified when the blades experience an increased Mach number while moving towards the observer position, and vice versa. The relative importance of the two mechanisms depends on the propeller operating point, with the unsteady blade loads only becoming dominant at the lowest thrust settings.

- Installation of the pylon adds a noise-generating mechanism, caused by the unsteady blade pressures resulting from the pylon-wake encounter. At sideslip, the associated noise penalty depended on the circumferential position of the wake encounter relative to the phase of the load oscillations due to the angle-of-incidence effects. The smallest increase in noise levels occurred when the wake was encountered in the part of the disk where the blade loads were at a minimum. The application of pylon trailing-edge blowing successfully decreases the noise penalty due to pylon installation, despite remaining non-uniformities in the blown wake profiles.

It has been shown that proper consideration of angular-inflow effects is crucial to minimize pylon–propeller interaction effects. Under asymmetric inflow conditions, significant benefits can be achieved in terms of both the aerodynamic and aeroacoustic performance of the propeller by selecting the optimal rotation direction.

Acknowledgments

The results presented in this paper were obtained by the APIAN-INF research partners in the framework of the transnational access program organized by the ESWIRP consortium, as part of the ESWIRP project (European Strategic Wind tunnels Improved Research Potential). The research leading to these results has received funding from the European Union Seventh Framework Programme (FP7-INFRASTRUCTURE-2008-1) under grant agreement n° 227816.

The authors would like to thank Hermann Holthusen for his efforts in the preparation and execution of the test campaign, and his assistance during the processing and analysis activities.

References

[1]Mann, S. and Stuart, C., "Advanced propulsion through the 1990s – An airframer's view," *AIAA/SAE/ASME/ASEE 21st Joint Propulsion Conference*, 1985, Monterey, CA, USA.

[2]Page, M. A., Ivey, D. M., and Welge, H. R., "Ultra High Bypass Engine Applications to Commercial and Military Aircraft," *SAE Technical Paper 861720*, 1986.

[3]Farokhi, S., "Pressure-Time History of Pylon Wake on a Pusher Propeller in Flight," *Journal of Propulsion and Power*, Vol. 6, No. 6, 1990, pp. 758–768.

[4]Farokhi, S., Taghavi, R., and Wetzel, K. K., "Frequency-Domain Analysis of Fluctuating Pressure on a Pusher Propeller Blade Surface," *Journal of Aircraft*, Vol. 31, No. 1, 1994, pp. 42–48.

[5]Block, P. J. W. and Gentry, Jr., G. L., "Directivity and Trends of Noise Generated by a Propeller in a Wake," *NASA-TP-2609*, 1986.

[6]Shivashankara, B., Johnson, D., and Cuthbertson, R., "Installation Effects on Counter Rotating Propeller Noise," *AIAA 13th Aeroacoustics Conference*, 1990, Tallahassee, FL, USA.

[7]Ricouard, J., Julliard, E., Omaïs, M., Regnier, V., Parry, A. B., and Baralon, S., "Installation effects on contra-rotating open rotor noise," *AIAA/CEAS 16th Aeroacoustics Conference*, 2010, Stockholm, Sweden.

[8]Paquet, C., Julliard, E., Genoulaz, N., Ricouard, J., and Spiegel, P., "Z08: low-speed aero-acoustic experimental characterization of open rotor installation on aircraft," *AIAA/CEAS 20th Aeroacoustics Conference*, 2014, Atlanta, GA, USA.

[9]Stürmer, A., Yin, J., and Akkermans, R., "Progress in aerodynamic and aeroacoustic integration of CROR propulsion systems," *The Aeronautical Journal*, Vol. 118, No. 1208, 2014, pp. 1137–1158.

[10]Gentry, G. L., Jr., Booth, E. R., Jr., and Takallu, M. A., "Effect of Pylon Wake With and Without Pylon Blowing on Propeller Thrust," *NASA-TM-4162*, 1990.

[11]Sinnige, T. and Veldhuis, L. L. M., "Pylon Trailing Edge Blowing Effects on the Performance and Noise Production of a Pusher Propeller," *AIAA 52nd Aerospace Sciences Meeting*, 2014, National Harbor, MD, USA.

[12]Sinnige, T., Lynch, K. P., Ragni, D., Eitelberg, G., and Veldhuis, L. L. M., "Aerodynamic and Aeroacoustic Effects of Pylon Trailing Edge Blowing on Pusher Propeller Installation," *AIAA/CEAS 21st Aeroacoustics Conference*, 2015, Dallas, TX, USA.

[13]Fernando, R. and Leroux, M., "Open-Rotor low speed aero-acoustics: wind tunnel characterization of an advanced blade design in isolated and installed configurations," *AIAA/CEAS 20th Aeroacoustics Conference*, 2014, Atlanta, GA, USA.

[14]Stürmer, A. and Yin, J., "Pylon Trailing Edge Blowing for the Control of CROR Unsteady Blade Loads," *New Results in Numerical and Experimental Fluid Mechanics VIII*, edited by A. Dillmann, G. Heller, H.-P. Kreplin, W. Nitsche, and I. Peltzer, Vol. 121 of *Notes on Numerical Fluid Mechanics and Multidisciplinary Design*, Springer Berlin Heidelberg, 2013, pp. 715–722.

[15]Magliozzi, B., "Noise Characteristics of a Model Counterrotating Prop-Fan," *AIAA 11th Aeroacoustics Conference*, 1987, Sunnyvale, CA, USA.

[16]Polacsek, C., Spiegel, P., Boyle, F., Eaton, J., Brouwer, H., and Nijboer, R., "Noise Computation of High-Speed Propeller-Driven Aircraft," *6th AIAA/CEAS Aeroacoustics Conference*, 2000, Lahaina, HI, USA.

[17]Bousquet, J.-M. and Gardarein, P., "Recent improvements in Propeller Aerodynamic computations," *AIAA 18th Applied Aerodynamics Conference*, 2000, Denver, CO, USA.

[18]Philipsen, I., Hoeijmakers, H., and Hegen, S., "An Overview of Advanced Propeller Simulation Tests in the German Dutch Wind Tunnels (DNW)," *AIAA 22nd Aerodynamic Measurement Technology and Ground Testing Conference*, 2002, St. Louis, MO, USA.

[19]Crozier, P., "APIAN Installed Tests in the ONERA S1MA Wind Tunnel," *AIAA 39th Aerospace Sciences Meeting & Exhibit*, 2001, Reno, NV, USA.

[20]Patterson, J. C., Jr. and Bartlett, G. R., "Effect of a Wing-Tip Mounted Pusher Turboprop on the Aerodynamic Characteristics of a Semi-Span Wing," *AIAA/SAE/ASME/ASEE 21st Joint Propulsion Conference*, 1985, Monterey, CA, USA.

[21]Hanson, D. B., "Sound from a Propeller at Angle of Attack: A New Theoretical Viewpoint," *Proceedings: Mathematical and Physical Sciences*, Vol. 449, No. 1936, 1995, pp. 315–328.